

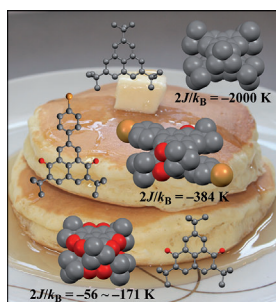
Radical π dimers: The crystal structures of 2,5-di-*tert*-butyl-6-oxophenalenoxyl (6OPO) stable neutral π radicals have been determined. In the crystal form, 8-*tert*-butyl- and 8-(*p*-XC₆H₄)-6OPO derivatives (X=I, Br) form π dimers (see figure) with weak intra-dimer antiferromagnetic exchange

interactions due to a small overlap of the singly occupied molecular orbitals. These overlapping modes are caused by both the topological symmetry of the spin density distribution of the 6OPO π radicals and the steric hindrance exerted by substituents in the molecular frameworks.

Radicals

S. Nishida, J. Kawai, M. Moriguchi,
T. Ohba, N. Haneda, K. Fukui,
A. Fuyuhiko, D. Shiomi, K. Sato,
T. Takui,* K. Nakasuji,
Y. Morita* ■■■■-■■■■

Control of Exchange Interactions in π Dimers of 6-Oxophenalenoxyl Neutral π Radicals: Spin-Density Distributions and Multicentered-Two-Electron Bonding Governed by Topological Symmetry and Substitution at the 8-Position

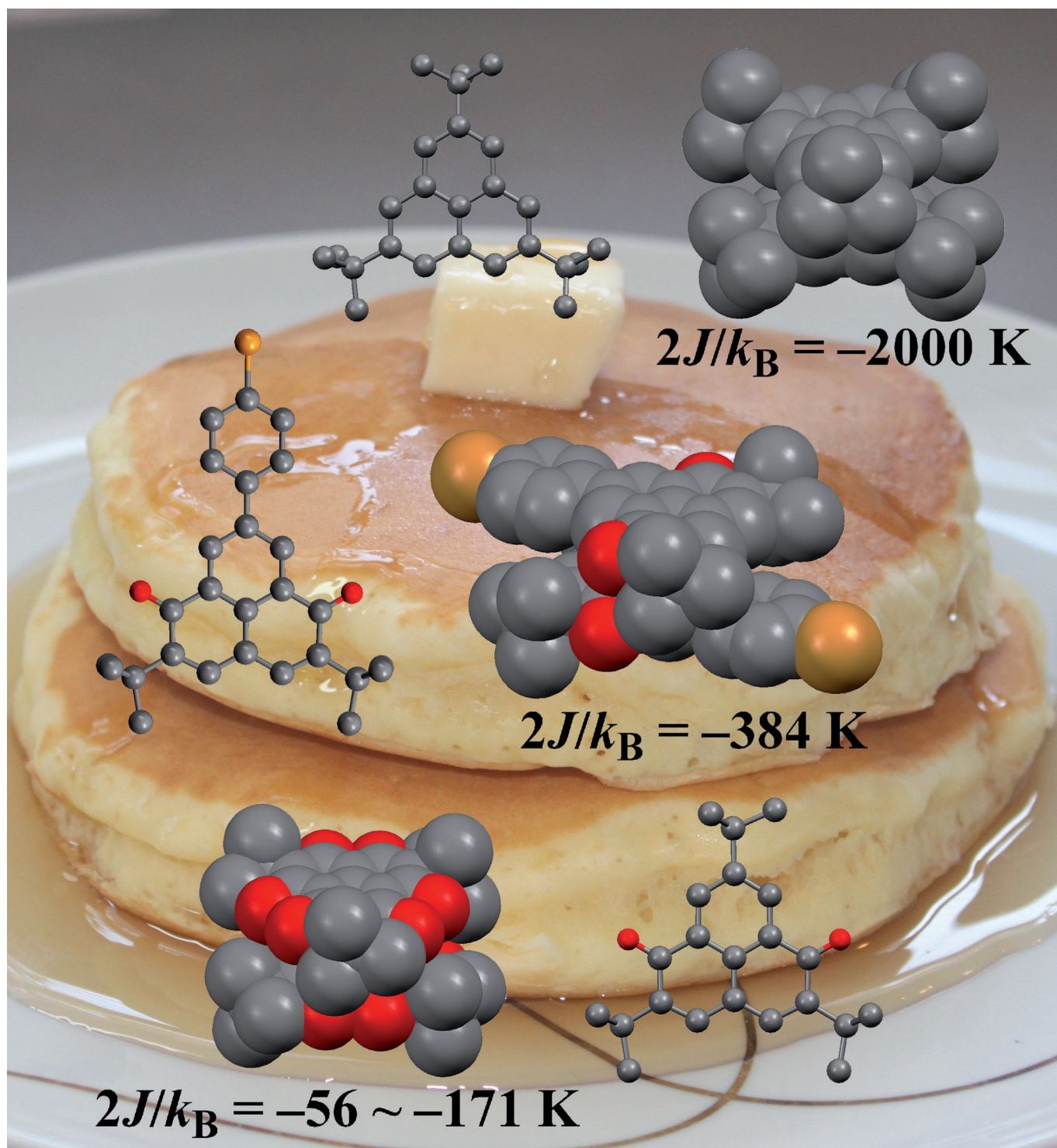


Radical π dimers

2,5-Di-*tert*-butyl-6-oxophenalenoxyl (6OPO) is a phenalenyl-based air-stable neutral π radical with extensive spin-delocalization, and 6OPO is a counter analogue of phenalenyl in terms of the topological symmetry of spin density distribution. SQUID measurements for 8-(*p*-BrC₆H₄)-6OPO showed that a weak antiferromagnetic exchange interaction occurs within the π -dimer. These results demonstrate that control in the spin distribution patterns of the phenalenyl skeleton switches the mode of exchange interaction within the phenalenyl-based π dimer. For more details see the Full Paper by T. Takui, Y. Morita et al. on page ■ ■ ff.

DOI: 10.1002/chem.201301783
Control of Exchange Interactions in π Dimers of 6-Oxophenalenoxyl Neutral π Radicals: Spin-Density Distributions and Multicentered–Two-Electron Bonding Governed by Topological Symmetry and Substitution at the 8-Position

Shinsuke Nishida,^[a, b] Junya Kawai,^[a] Miki Moriguchi,^[a] Tomohiro Ohba,^[a]
Naoki Haneda,^[a] Kozo Fukui,^[a] Akira Fuyuhiko,^[a] Daisuke Shiomi,^[c] Kazunobu Sato,^[c]
Takeji Takui,^{*[c]} Kazuhiro Nakasuji,^[a] and Yasushi Morita^{*[a, b]}



Abstract: The tri-*tert*-butylphenalenyl (TBPLY) radical exists as a π dimer in the crystal form with perfect overlapping of the singly occupied molecular orbitals (SOMOs) causing strong anti-ferromagnetic exchange interactions. 2,5-Di-*tert*-butyl-6-oxophenalenoxyl (6OPO) is a phenalenyl-based air-stable neutral π radical with extensive spin delocalization and is a counter analogue of phenalenyl in terms of the topological symmetry of the spin density distribution. X-ray crystal structure analyses showed that 8-*tert*-butyl- and 8-(*p*-XC₆H₄)-6OPOs (X=I, Br) also

form π dimers in the crystalline state. The π -dimeric structure of 8-*tert*-butyl-6OPO is seemingly similar to that of TBPLY even though its SOMO–SOMO overlap is small compared with that of TBPLY. The 8-(*p*-XC₆H₄) derivatives form slipped stacking π dimers in which the SOMO–SOMO overlaps are greater than in 8-*tert*-butyl-6OPO,

but still smaller than in TBPLY. The solid-state electronic spectra of the 6OPO derivatives show much weaker intradimer charge-transfer bands, and SQUID measurements for 8-(*p*-BrC₆H₄)-6OPO show a weak antiferromagnetic exchange interaction in the π dimer. These results demonstrate that the control of the spin distribution patterns of the phenalenyl skeleton switches the mode of exchange interaction within the phenalenyl-based π dimer. The formation of the relevant multicenter–two-electron bonds is discussed.

Keywords: absorption • density functional calculations • magnetic properties • radicals • X-ray diffraction

Introduction

The control of intermolecular exchange interactions between stable organic open-shell molecules^[1] is a crucial issue in the design and development of molecule-based magnetic materials.^[2] Molecular design approaches to the establishment of stronger ferromagnetic exchange interactions within molecular open-shell entities, such as molecular high spins, have been well tested from both theoretical and experimental sides.^[2c] Recent trends in open-shell chemistry are towards the weakening of exchange coupling leading to electromagnetic control of molecular spins for spin qubits (quantum bits) in quantum computing/quantum information technology (QC/QIP).^[3] On the one hand, magnetic properties such as intramolecular exchange couplings and magnetic tensors of organic open-shell systems strongly depend on individual molecular/electronic structures, and their molecular design has been well underlain by quantum chemistry. On the other hand, the control of intermolecular exchange couplings between organic open-shell entities in solids is still a challenging issue in chemistry and materials science. In particular, the coupling modes as well as the magnitude of the

coupling cannot be fully understood, nor controlled. In this context, exchange interactions based on multicentered bonds in π dimers are of importance.^[4]

Phenalenyl is a neutral hydrocarbon π radical with extensive spin delocalization on the six α -carbon atoms.^[5,6] This π radical easily forms a σ -dimer and reacts with oxygen, but high air-stability can be acquired by introducing steric protection around the molecular framework through bulky substituents (tri-*tert*-butylphenalenyl, TBPLY^[7]). In the crystalline state, TBPLY forms a π dimer that adopts a staggered arrangement of the *tert*-butyl groups so as to avoid steric repulsion.^[8,9] We first discovered the existence of a 12-center–2-electron long C–C bond^[6,10,11] through the perfect overlap of singly occupied molecular orbitals (SOMOs, Figure 1a), which gives rise to a strong antiferromagnetic intermolecular exchange interaction within the π dimer ($2J/k_B = -2000$ K).^[7] This multicenter bond^[4] features the dynamic physical phenomena of phenalenyl-based neutral π radicals; TBPLY shows thermochromism in solution induced by the thermal equilibrium between the π dimer and π radical monomer,^[6,10] and zwitterionic bis-phenalenyl–boron complexes exhibit magneto-optical-electronic bistability in the crystalline state through a change in the electronic interactions within the π -dimeric structures with temperature.^[12] Furthermore, the crystal of tri-*tert*-butyl-1,3-diazaphenalenyl^[13] shows a continuous change in color with temperature due to the equilibrium between a π dimer similar to TBPLY and a σ -dimer.^[14]

Among the phenalenyl-based π radicals that we have designed and synthesized in the past two decades,^[6] 2,5-di-*tert*-butyl-6-oxophenalenoxyl (6OPO)^[6,15,16] is an air-stable neutral π radical possessing two oxygen atoms on the phenalenyl skeleton as both a heteroatomic chemical modification and an extension of the π conjugation (Figure 1b, R=H). Notably, 6OPO exhibits extensive spin delocalization similar to phenalenyl, although this π radical is different to phenalenyl (Figure 1b) in terms of the topological symmetry of spin density distribution.^[6,15,17] Furthermore, two-electron re-

[a] Dr. S. Nishida, Dr. J. Kawai, M. Moriguchi, T. Ohba, N. Haneda, Dr. K. Fukui, Prof. A. Fuyuhiko, Prof. K. Nakasuji, Prof. Y. Morita
Department of Chemistry, Graduate School of Science
Osaka University, Toyonaka, Osaka 560-0043 (Japan)
Fax: (+81) 6-6850-5395
E-mail: morita@chem.sci.osaka-u.ac.jp

[b] Dr. S. Nishida, Prof. Y. Morita
Core Research for Evolutional Science and Technology (CREST)
Japan Science and Technology Agency (JST)
5 Sanban-cho, Chiyoda-ku, Tokyo 102-0075 (Japan)

[c] Prof. D. Shiomi, Prof. K. Sato, Prof. T. Takui
Department of Chemistry, Graduate School of Science
Osaka City University, Sumiyoshi-ku, Osaka 558-8585 (Japan)
Fax: (+81) 6-6605-2522
E-mail: takui@sci.osaka-cu.ac.jp

Supporting information for this article is available on the WWW under <http://dx.doi.org/10.1002/chem.201301783>.

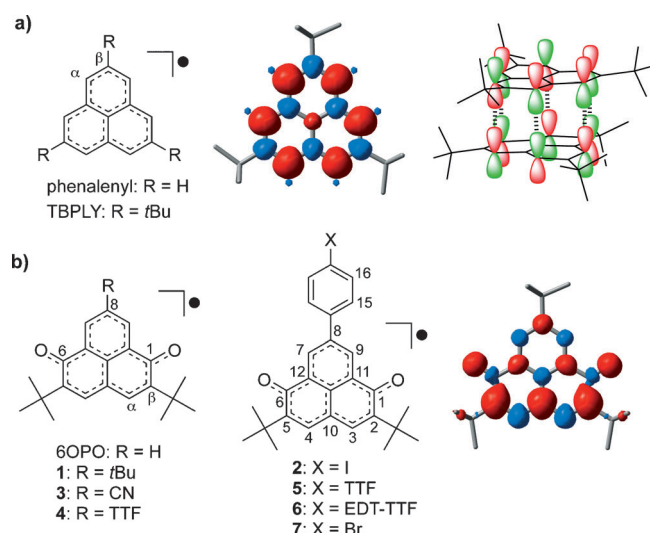


Figure 1. a) Phenalenyl derivatives (left), the spin density distribution of TBPLY (center), illustration of a 12-center-2-electron long C–C bond with perfect SOMO–SOMO overlap in the π dimer of TBPLY (right). b) 8-Substituted 6OPOs (left and center) and the spin density distribution of **1** (right). Red and blue regions denote positive and negative spin densities, respectively. The spin density distributions were calculated by DFT at the UB3LYP/6-31G(d,p)//UB3LYP/6-31G(d,p) level of theory.

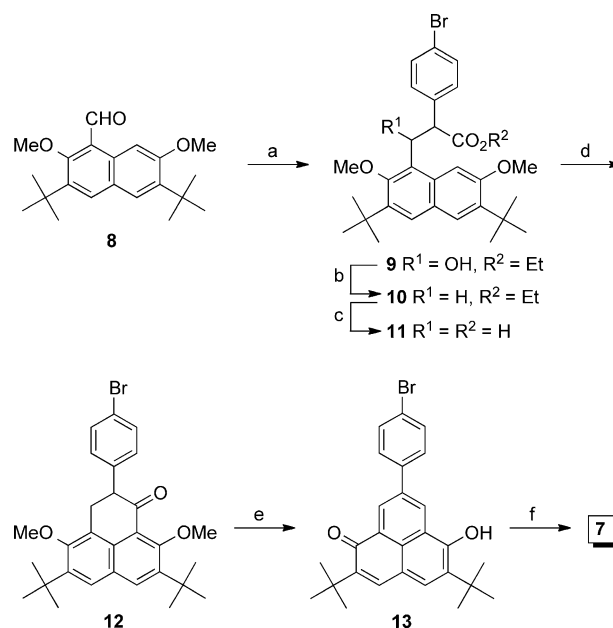
duction of this π radical gives the corresponding radical dianion species with high stability in a degassed solution, the spin structure of which is remarkably different to that of the neutral species.^[6,18] These unique spin properties suggest that 6OPO is an inherently different organic neutral π radical to phenalenyl and simple aroxyl radicals, thereby providing new insights into open-shell chemistry. Substitution at the 8-position with a *tert*-butyl group (**1**; Figure 1b)^[6,15] or a *p*-IC₆H₄ group (**2**; Figure 1b)^[19] further increases the stability of the neutral π radicals. We have recently synthesized and isolated 8-CN-6OPO (**3**) with a stability comparable to **1** and **2** despite low steric protection of the 8-position.^[20] In the quest for novel multifunctional molecular spin systems,^[21] electron-donor-substituted 6OPOs **4**,^[22] **5**,^[19b] and **6**^[19b] have been designed and synthesized. Interestingly, the π radical **4** shows “spin-center transfer” accompanying solvato/thermochromism caused by intramolecular electron transfer controlled by solvent and temperature.^[22] Moreover, use of the two-stage redox ability of **1** to charge/discharge afforded high-capacity rechargeable batteries, “molecular spin batteries”.^[23] These studies demonstrated that 6OPO is a promising building block for next-generation molecular functional materials.

In this study we have discovered that **1**, **2**, and 8-(*p*-BrC₆H₄) derivative **7** form π dimers in their crystal forms by X-ray crystal structure analyses. On the basis of these structures, electronic absorption spectra, and superconducting quantum interference device (SQUID) measurements, and with the help of density functional theory (DFT),^[24] we illustrate that the magnitude of the antiferromagnetic exchange coupling is governed by the topological symmetry of the spin density distribution over the phenalenyl skeleton and

the electronic structure of the substituent at the 8-position.^[25] We emphasize that π -layered packing modes can be used to develop molecular functional materials in a controllable manner.

Results and Discussion

Synthesis and electronic-spin structure of the neutral π radical **7:** The neutral π radical **7** was synthesized from a 1-formylnaphthalene derivative **8**^[15] in six steps (Scheme 1). The aldol condensation reaction of **8** with the zinc enolate generated from ethyl (4-bromophenyl)acetate with lithium diisopropylamide (LDA) followed by the addition of ZnCl₂



Scheme 1. Synthesis of the neutral π radical **7**. Reagents and conditions: a) LDA, ZnCl₂, 4-BrC₆H₄CH₂CO₂Et, THF, –78 °C, 80%; b) Et₃SiH, CF₃CO₂H, CH₂Cl₂, RT, 96%; c) KOH, EtOH/H₂O, 100 °C, 75%; d) i. (COCl)₂, 65 °C; ii. AlCl₃, CH₂Cl₂, –78 °C, 78%; e) i. LiAlH₄, THF, RT; ii. LiI, hexamethylphosphoric triamide (HMPA), 170 °C, 52%; f) PbO₂, benzene, RT, quant.

quantitatively gave hydroxy ester **9**. Reductive elimination of the hydroxy group of **9** and subsequent hydrolysis of the ethyl ester **10** afforded carboxylic acid derivative **11**. The acid derivative **11** was converted into phenalanone derivative **12** by Friedel–Crafts cyclization. The carbonyl group of **12** was reduced and subsequently subjected to demethylation and autoxidation to give 6-hydroxyphenalenone **13**. Oxidation of **13** with PbO₂ yielded **7** as a neutral π radical that is highly stable to air in the solid state for a long period of time.

The electronic-spin structure of **7** was studied by EPR and electron-nuclear multiple magnetic resonance (¹H ENDOR/TRIPLE) spectroscopy at 290 K in toluene (3.6 × 10^{–5} M). Figure 2a shows the EPR spectrum of **7** with

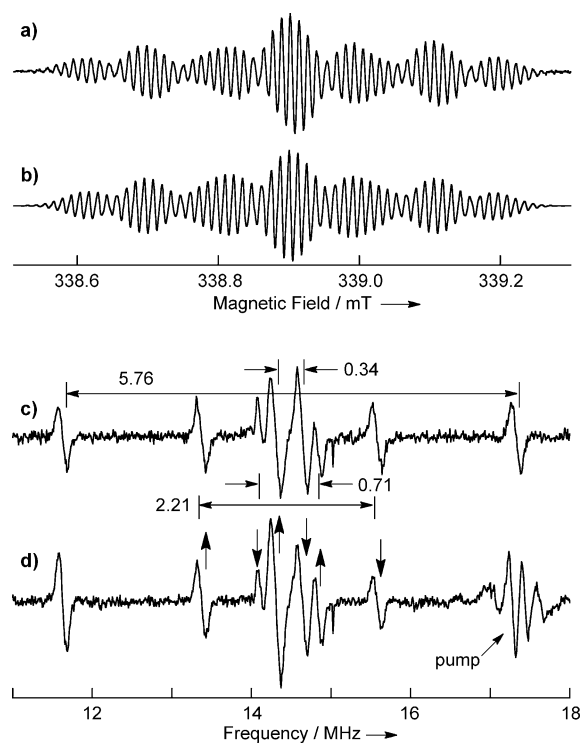


Figure 2. a) Observed cw-EPR spectrum of **7** (microwave frequency, 9.521982 GHz; field modulation, 12.5 kHz, which was used to eliminate the effects of a side-band production due to 100 kHz field modulation) and b) the corresponding simulated spectrum. c) ^1H ENDOR and d) TRIPLE (pump frequency, 17.33 MHz) spectra recorded at 290 K for **7** in toluene ($3.6 \times 10^{-5} \text{ M}$). The g value was determined experimentally to be 2.0045. In (d), the vertical upward and downward arrows denote the increase and decrease in ENDOR intensity at the resonance frequency during the pumping in TRIPLE spectroscopy. The TRIPLE experiment directly gives information on the relative signs of the four kinds of protons (hfcc: $a = 0.71, 0.34, 2.21, 5.76$ MHz; see Figure 3a, in which the hfccs are given in units of mT with $g = 2.0045$).

well-resolved hyperfine structures with a g value of 2.0045. ^1H ENDOR/TRIPLE spectroscopy enabled us to determine precisely the hyperfine coupling constants (hfccs) of the protons and their relative signs (Figures 2c,d, and 3a). The signs of the hfccs give crucial information on the identity of radicals and on their electronic structures. A satisfactory EPR spectral simulation was achieved on the basis of the hfccs obtained from ^1H ENDOR/TRIPLE spectroscopy. The spin density distribution of **7** was calculated by DFT at the UB3LYP/6-31G(d,p)//UB3LYP/6-31G(d,p) level of theory. Figure 3b shows extensive spin delocalization of **7** similar to that of **2**.^[19a]

X-ray crystal structure analysis of 1, 2, and 7: Single crystals of **1**, **2**, and **7** were obtained by recrystallization from degassed solutions in sealed tubes (hexane at -20°C for **1**, hexane/acetonitrile at 4°C for **2**, and $\text{CHCl}_3/\text{acetone}$ at -20°C for **7**). Figure 4 shows the molecular structures of **1**, **2**,^[26] and **7**^[27] determined by X-ray diffraction analysis. Compound **1** is statistically disordered in the crystal, showing a crystallographic three-fold rotation axis. Thus, the oxygen

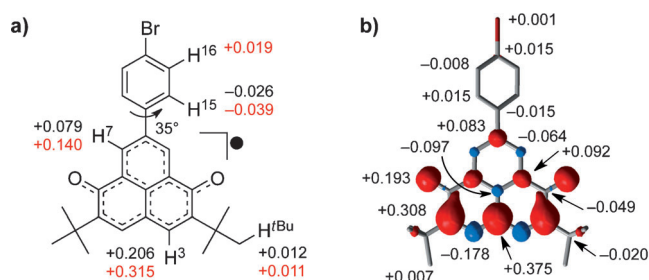


Figure 3. a) Observed (black numerals) and calculated hfccs (red numerals) of **7**. The hfccs were determined by ^1H ENDOR/TRIPLE spectroscopy. The hfcc of 16-H was not determined experimentally. b) Calculated spin density distribution of **7**. The dihedral angle between the $p\text{-BrC}_6\text{H}_4$ and 6OPO moieties is 35° . The red and blue regions denote positive and negative spin densities, respectively. The calculation was carried out at the UB3LYP/6-31G(d,p)//UB3LYP/6-31G(d,p) level of theory.

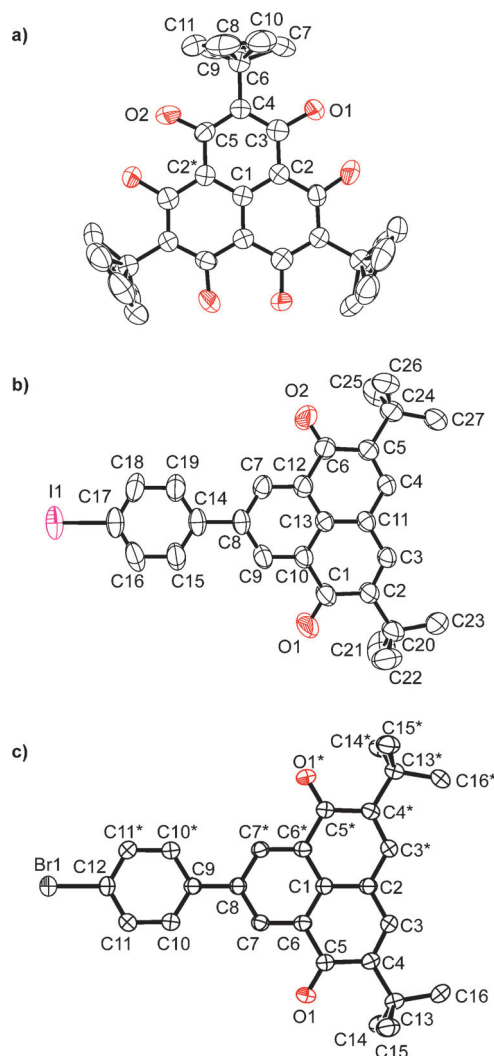


Figure 4. ORTEP representations of a) **1**, b) **2**, and c) **7**. For clarity, the hydrogen atoms of the π radicals and of acetonitrile and acetone molecules contained in the crystals of **2** and **7**, respectively, as solvents of crystallization have been omitted. Thermal ellipsoids are drawn at the 50% probability level.

atoms of **1** are located at the α sites of the phenalenyl skeleton and refined with occupancy factors of $1/3$ and $2/3$ for oxygen and hydrogen atoms, respectively. The *tert*-butyl groups possess two conformations depending on the positions of the oxygen atoms (C6–C10–C11–C12 for O1 and C6–C7–C8–C9 for O2), which were refined with an occupancy factor of $1/2$ (Figure 4a, Figure S1).

Such disorder is not found in the crystals of **2** and **7**, which enables us to discuss precisely their molecular structure (Figure 4b,c, and Figures S3 and S4 in the Supporting Information). The bond equalization of 1.38–1.40 Å observed for the C–C bonds in the six-membered ring systems of **2** (C7–C8–C9–C10–C13–C12) and **7** (C1–C6–C7–C8–C7*–C6*) in the 6OPO skeletons gives experimental evidence for local aromaticity^[28] in these ring systems; this is consistent with our previous studies in terms of quantitative resonance structures based on the molecular-orbital (MO)-based valence bond (VB) method^[20,29] and nucleus-independent chemical shift (NICS) calculations.^[17] In addition, the *p*-BrC₆H₄ moiety is co-planar with the 6OPO moiety, which contrasts with the optimized structure calculated by the DFT method (Figure 3a). However, theoretical calculations indicate a negligible difference in spin density distribution between the X-ray and calculated optimized geometries (see Figure S2).

The π radical **1** forms a π dimer in an arrangement that at first sight is similar to that of TBPLY (Figure 5a). A closer study indicates that the interplanar distance in the π dimer of **1** (3.49–3.55 Å) is longer than that in TBPLY (3.201(8)–3.323(6) Å).^[17] Importantly, both this long intradimer distance and the topological symmetry of the spin density distribution of the monomer π radical (Figure 1b)

cause a smaller SOMO–SOMO overlap within the π dimer compared with that in TBPLY.

The π radicals **2** and **7** form similar π dimers, but in a slipped stacking motif that differs from that of **1** (Figure 5b,c). In these π dimers, there are overlaps at the 8-, 10-, 11-, and 12-carbon atoms and two oxygen atoms (numbering is shown in Figure 1b), on which sizable spin densities reside. The interplanar distances are 3.36–3.43 and 3.38–3.51 Å for the π dimers of **2** and **7**, respectively, which are shorter than those of **1**. The observed slipped stacking structures arise from both the effect of electronic stabilization by the intermolecular overlap interaction and steric repulsion due to the *tert*-butyl groups at the 2,5-positions.

The arrangement and interdimer interactions of the π dimers of **1**, **2**, and **7** are shown in Figure 6. The oxygen atoms of the π dimers of **1** are in close contact (Figure 6a and Figure S5 in the Supporting Information).^[30] In contrast, the π dimers of **2** and **7** form one-dimensional columnar structures. The π dimers of **2** stack in a head-to-tail manner along the *b* axis with an interdimer distance of 3.47–3.56 Å (Figure 6b and Figure S6). These columns make contact through the iodine atoms. The π dimers of **7** stack along the *a* axis with an interdimer distance of 3.64–3.69 Å (Figure 6c

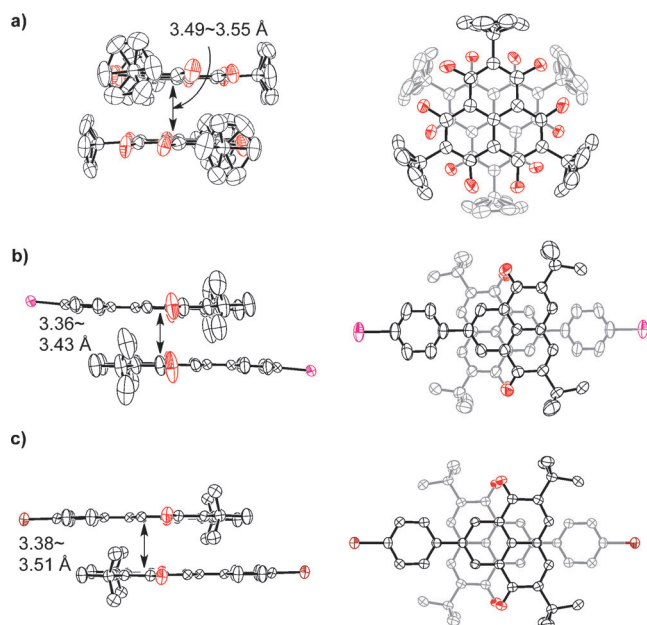


Figure 5. Side views (left) and top views (right) of the π dimers of a) **1**, b) **2**, and c) **7**. The numbers denote interplanar distances in the π dimers. Thermal ellipsoids are drawn at the 50% probability level.

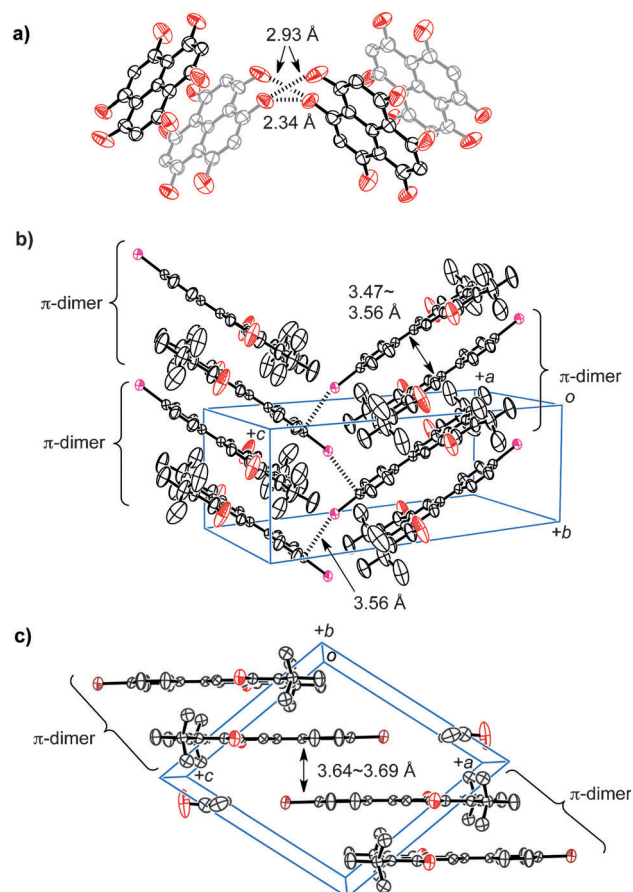


Figure 6. a) Interdimer interactions between the oxygen atoms of **1**. Packing diagrams of b) **2** (acetonitrile molecules as solvent of crystallization have been omitted for clarity) and c) **7**. Thermal ellipsoids are drawn at the 50% probability level.

and Figure S7) within the column, which is much longer than the intradimer distance. These columns are discrete from each other. In the crystals of **2** and **7**, acetonitrile and acetone molecules occupy the spaces between the columns of the π dimers as solvents of crystallization, respectively. The results of the X-ray analyses demonstrate that the substituent at the 8-position of 6OPO plays an important role in controlling intra- and interdimer interactions.

To examine the SOMO–SOMO overlap of these π dimers, we calculated the SOMOs of **1** and **7** by DFT calculations at the UB3LYP/6-31G(d,p) level of theory. The molecular geometries used in these calculations were those determined by X-ray crystal structure analysis in the case of **7**, and by DFT calculations in the case of **1** owing to the disorder in the crystal of the molecule. Figure 7a shows that the coefficients of the SOMOs mainly exist on the 1-, 2-, 5-, 6-, 8-, 10-, 11-, and 12-carbon atoms and the two oxygen atoms in the molecules of **1** and **7** (see also Figure 1b).

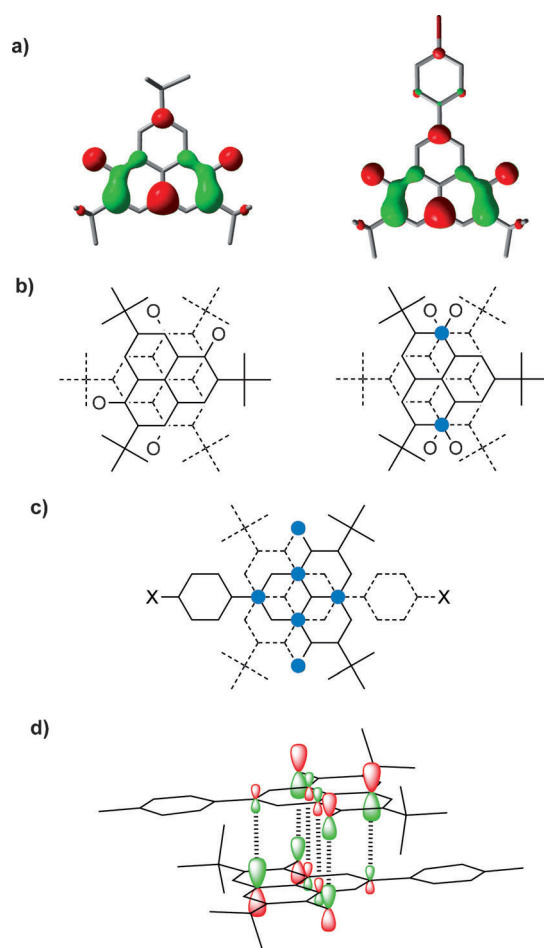


Figure 7. a) SOMOs of **1** (left) and **7** (right) calculated at the UB3LYP/6-31G(d,p) level of theory. The molecular geometries used for the calculations were the optimized structure of **1** and the X-ray crystal structure of **7**. Illustrations of possible modes of overlap for the π dimers of b) **1** and c) **7**. d) Schematic diagram of the SOMO–SOMO overlap in the π dimers of **7**. Blue filled circles in (b) and (c) denote the positions at which the SOMOs overlap.

The disorder in the π dimer of **1** has two possible orientations, one rotated away from the eclipsed conformation by 60° and the other by 180° around the three-fold rotation axis (Figure 7b). The 60° conformer has no SOMO–SOMO overlap (Figure 7b, left), whereas in the 180° conformer, the 1,6-carbon atoms with small coefficients of the SOMO can be superimposed (Figure 7b, right). However, the SOMO–SOMO overlap is assumed to be small because the interplanar distance (Figure 5a) is longer than the sum of the van der Waals radii of carbon atoms (3.40 \AA). These results indicate that the existence of a multicenter–two-electron C–C bonding interaction is negligible in the π dimer of **1**.

In sharp contrast to the π dimer of **1**, in the case of the π dimer of **7**, the SOMO–SOMO overlap at the 8-, 10-, 11-, and 12-carbon atoms and the two oxygen atoms with large coefficients of the SOMO (Figure 7c). This mode of overlap implies a multicenter–two-electron long C–C bond in the π dimer, although the bonding interaction is weaker than that in TBPLY. The difference in the intradimer interaction between the π dimers of TBPLY and **1** is ascribable to the topological symmetry of the spin density (also SOMO) distribution of the monomer π radicals,^[31] and the difference between the π dimers of **1** and **7** (and **2**) is caused by the steric hindrance of the substituents at the 8-position.

Electronic absorption spectra of 1, 2, and 7: To understand the intermolecular electronic interactions, we recorded the electronic absorption spectra of **1**, **2**, and **7** in hexane solutions and as KBr pellets of powders. The π radical **1** shows a weak absorption band with a maximum at 642 nm in solution, ascribed to intramolecular transitions. In the solid state, a weak band centered at 642 nm and an additional broad band between 800 and 900 nm are observed. The latter low-energy broad band is presumably due to an intermolecular charge-transfer (CT) transition because similar low-energy bands appear in the electronic absorption spectra of π dimers of organic open-shell molecules,^[32] including phenalenyl-based neutral radicals.^[6,7,10,13,14] The intensity of the CT band is lower than that of TBPLY,^[6,7,10] which implies weak electronic interactions within the π dimer in the solid state. Quantum chemical calculations for these absorption bands are underway.

The π radical **2** shows a weak broad band with a maximum at 651 nm due to intramolecular transitions in solution similar to **1** (Figure 8b). The spectrum of **2** in a KBr pellet exhibits a broad band between 800 and 1000 nm, which is ascribable to intermolecular CT transitions. The CT band is also much weaker than that of TBPLY, which indicates a weak electronic interaction within the π dimer owing to the small SOMO–SOMO overlap in comparison to that of TBPLY.

The π radical **7** shows similar spectra to **2** (Figure 8c), which is consistent with the similarity in the π -dimeric structures of **2** and **7**. In addition, temperature-dependent electronic absorption spectra of **7** in CH_2Cl_2 were recorded that showed fairly small spectral changes with temperature (see Figure S8 in the Supporting Information). This result is in

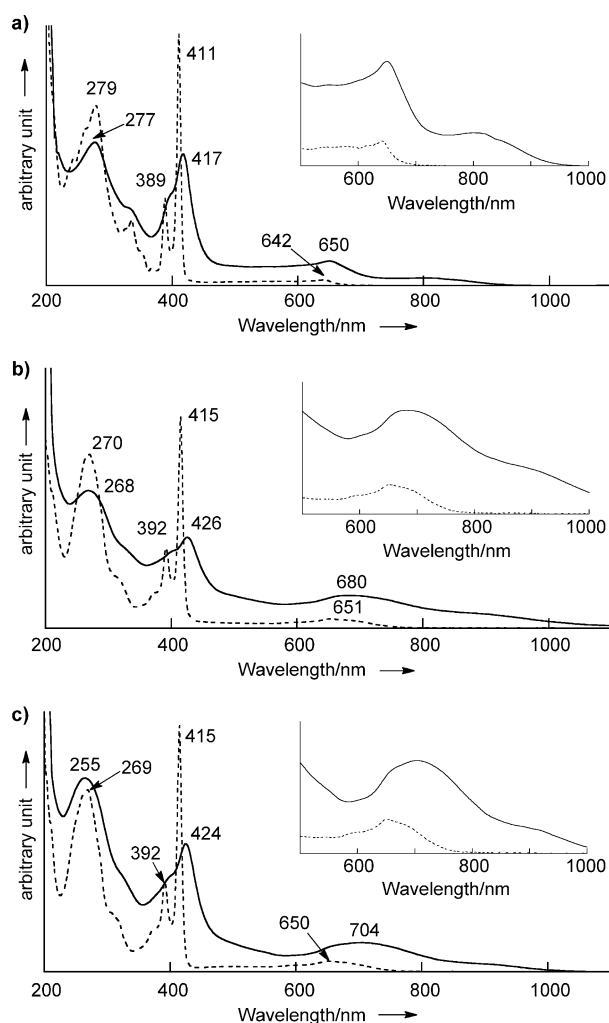


Figure 8. Electronic absorption spectra of a) **1**, b) **2**, and c) **7**. Broken and solid lines denote samples in hexane solutions and KBr pellets, respectively. Concentrations of the π radicals in hexane: 8.0×10^{-5} M **1**, 8.0×10^{-5} M **2**, and 8.6×10^{-5} M **7**. Insets: Enlargements of the spectra in the region between 500 and 1000 nm.

sharp contrast to that of TBPLY, which shows a new absorption band at low temperature due to the formation of a π dimer in solution.^[10]

Magnetic properties of 7: To evaluate the intradimer exchange interaction of the 6OPO derivatives, the bulk magnetic properties of crystals of **7** were examined by SQUID measurements in the temperature range of 1.8–298 K at 0.1 T (Figure 9). The data were corrected for the diamagnetic contribution of $\chi_d = -230 \times 10^{-6} \text{ emu mol}^{-1}$, calculated by Pascal's method. The magnetic behavior observed can be approximately interpreted by using a model comprising a singlet ground state and a triplet state lying above the ground state by 384 K ($= 2J/k_B$). The theoretical curves were calculated by using Equation (1) in which the first term represents the ground-state singlet dimer of **7** with the antiferromagnetic interaction J and the second term corresponds to magnetically independent molecules without the formation

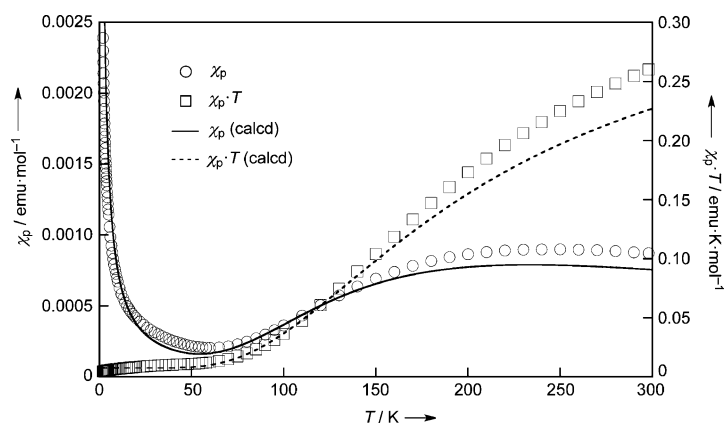


Figure 9. Temperature dependence of χ_p (circles) and $\chi_p T$ (squares) of **7**-((CH₃)₂CO) vs. T . The best-fit parameters reproducing the observed $\chi_p T$ curves are $2J/k_B = -384$ K, $\alpha = 0.02$, the ratio of diamagnetic impurity, and $g = 2.005$. The observed departure from the theoretical curves above 140 K is noticeable and a possible reason is given in the text.

of the π dimer in a lattice defect. The parameter α denotes the ratio of impurity ($S = 1/2$) from the defects. The symbols N , g , μ_B , and k_B represent Avogadro's constant, the g factor, the Bohr magneton, and the Boltzmann constant, respectively.

$$\chi_p = (1 - 2\alpha)(2g^2\mu_B^2/k_B T) / [3 + \exp(-2J/k_B T)] + \alpha N g^2 \mu_B^2 / 4k_B \quad (1)$$

Above 140 K the observed χ_p values deviate upward from the theoretical curve, which was calculated with $2J/k_B = 384$ K, $\alpha = 0.02$, and $g = 2.005$.^[33,34] We noted that such deviations appeared for different samples. We assume that one of the causes of this behavior is the partial, gradual vaporization of the acetone contained in the crystals of **7** during the SQUID measurements. The vaporization was found to be accelerated at higher temperatures. The measurements from room temperature to 350 K showed an irreversible increase in χ_p at around 330 K associated with a loss in weight, giving support to the above-mentioned assumption: The boiling point of bulk acetone is 329 K. These results demonstrate a smaller antiferromagnetic interaction within the π dimers of **7** ($2J/k_B = -384$ K, corresponding to the singlet–triplet energy separation) than that in TBPLY ($2J/k_B = -2000$ K^[7]), being consistent with the smaller SOMO–SOMO overlap within the π dimers of **7**. Thus, considering the smaller SOMO–SOMO overlap in **1**, the antiferromagnetic interaction within the π dimers of **1** is expected to be smaller than that within the π dimers of **7**.^[35]

The $2J/k_B$ values of the π dimers of **1** and **7** were estimated by using the DFT method^[36] (see Figures S9–S13 in the Supporting Information). At the UB3LYP/6-31G(d) level of theory, the calculations predicted a singlet diradical character in the π dimers of **1** with a $2J/k_B$ value of -56.2 to -171.2 K. The orbital overlap (T) between magnetic orbitals

was estimated to be 0.00504–0.0891 for **1** by natural orbital analyses. These results give support to the small SOMO–SOMO overlap within the π dimer of **1**. The negative exchange interaction is interpreted in terms of antiferromagnetic spin polarization effects traveling through the α -carbon atoms with negative spin densities. The calculations were also carried out for the π dimers of **7**, which show singlet diradical character with $2J/k_B$ values of -424 K and T values of 0.1674, in good agreement with the experimental value.

Conclusion

In this work we have determined the molecular and π -dimeric structures of the 6OPO derivatives **1**, **2**, and **7** by means of X-ray crystal structure analyses and revealed the occurrence of relevant weak intradimer exchange interactions. The π dimer of 8-*tert*-butyl-6OPO (**1**) in the crystalline state has an arrangement similar to that of TBPLY, although the exchange interaction is smaller due to both the topological symmetry of the spin density distribution (SOMOs) of the monomer π radical and the fairly long interplanar distance within the π dimer. The 8-(*p*-IC₆H₄) and 8-(*p*-BrC₆H₄) derivatives **2** and **7**, respectively, form slipped stacking π dimers due to lower steric repulsion around the 8-positions in comparison with **1**. The SOMO–SOMO overlap within the π dimers are larger than that in **1**, however, the exchange interactions are still much smaller than those of TBPLY.

These results demonstrate that the topological symmetry of spin density (also SOMO) distribution and steric hindrance of the substituent at the 8-position play a vital role in controlling the intermolecular exchange interactions of spin-delocalized neutral π radicals.^[2,37] To develop novel multifunctional materials comprising stable organic π radicals, it is necessary to build up intermolecular networks with multidimensional intermolecular interactions in a controlled manner. In this context, we have noted that exchange interactions based on multicentered–two-electron C–C long bonds in π dimers are of importance in assembling neutral π radicals in the solid state. Detailed theoretical studies of multicentered–two-electron C–C bond formation in the π dimers are underway. We have recently reported bowl-shaped stable neutral π radicals,^[38] helicene-structured π radicals,^[39] and π -extended radicals^[40] as building blocks of multidimensional networks through π – π interactions. The results of this study will open up new avenues to control intermolecular exchange interactions in multidimensional networks in terms of the topological symmetry of spin density distribution, strongly relevant to the SOMOs of the building blocks, and importantly contribute to the application of molecule-based magnetic materials,^[2] molecular-spin qubits for QC/QIP,^[3] and molecular spin batteries.^[23]

Experimental Section

¹H NMR spectra were recorded at 270 MHz on a JEOL JNM-EX270 FT-NMR with CDCl₃ or [D₆]DMSO as solvent and Me₄Si or residual solvent as internal standard. IR spectra were recorded on a Perkin-Elmer 1640 FT-IR by using KBr pellets or in Cl₂C=CCl₂ solution. X-band liquid-phase EPR and ¹H ENDOR/TRIPLE spectra were recorded on Bruker EPR ESP300 and ENDOR ESP350 spectrometers by using sample solutions degassed by using the freeze–pump–thaw method prior to the measurements. The static magnetic susceptibility was measured with a Quantum Design MPMS2 SQUID magnetometer with an applied field of 0.1 T in the temperature range of 1.8–298 K. Electronic absorption spectra were recorded on a SHIMADZU UV-3100PC in hexane solutions or KBr pellets for measurements at room temperature, and in CH₂Cl₂ for variable-temperature measurement. EI-MS was performed on a SHIMADZU QP-5000 at 70 eV. X-ray crystallographic measurements on single crystals were made by using a Rigaku RAXIS RAPID Imaging Plate and graphite-monochromated MoK α radiation ($\lambda=0.71075$ Å). These structures were solved by direct methods and refined by full-matrix least-squares techniques (SHELXS-97).^[41] Melting points were measured with a hot-stage apparatus without correction. Elemental analyses were performed at the Graduate School of Science, Osaka University. TLC was performed on E. Merck precoated (0.25 mm) silica gel 60 F₂₅₄ plates. The plates were sprayed with a solution of 10% phosphomolybdic acid in 95% EtOH and then heated until the spots became clearly visible. Silica gel 60 (100–200 mesh) was used for column chromatography. Solvents were dried (drying agent in parentheses) and distilled under argon prior to use: THF (Na benzophenone ketyl), hexamethylphosphoric triamide and CH₂Cl₂ (CaH₂), Cl₂C=CCl₂ (P₄O₁₀). Ethyl (4-bromophenyl)acetate was prepared by esterification of purchased (4-bromophenyl)acetic acid with EtOH in the presence of a catalytic amount of conc. H₂SO₄. 2,5,8-Tri-*tert*-butyl-6-oxophenalenoxyl (**1**),^[15] 8-(*p*-iodophenyl)-2,5-di-*tert*-butyl-6-oxophenalenoxyl (**2**),^[19] 3,6-di-*tert*-butyl-2,7-dimethoxynaphthalene-1-carbaldehyde (**8**),^[15] and active PbO₂^[42] were prepared according to literature methods. All reactions requiring anhydrous conditions were conducted under argon.

Syntheses

Ethyl 2-(4-bromophenyl)-3-(3,6-di-*tert*-butyl-2,7-dimethoxynaphthalen-1-yl)-3-hydroxypropanoate (**9**): Diisopropylamine (9.0 mL, 64.2 mmol) was dissolved in THF (150 mL) in a 500 mL round-bottomed flask and cooled to -78 °C under argon. *n*BuLi (1.6 M hexane solution, 39.0 mL, 61.0 mmol) was added to the mixture and stirred for 1 h. Ethyl (4-bromophenyl)acetate (45.9 g, 189 mmol) was added and the mixture stirred for 1 h. Then ZnCl₂ (8.60 g, 63.1 mmol) was added to the reaction mixture and stirred for 1 h. After the addition of the 1-formynaphthalene derivative **8** (5.00 g, 15.2 mmol) in one portion, the mixture was stirred for 2 h. It was then poured into a 2 M HCl aqueous solution (100 mL) and extracted with ethyl acetate. The organic extracts were dried over Na₂SO₄, filtered, and concentrated under reduced pressure. The residue was subjected to silica gel column chromatography with a 10:1–2:1 mixture of hexane and ethyl acetate as eluent to give **9** (6.96 g, 80%) as a yellow solid. M.p. 83–84 °C; $R_f=0.16$ (5:1 hexane/ethyl acetate); ¹H NMR (270 MHz, CDCl₃): $\delta=1.17$ (s, 9H), 1.45 (s, 9H), 1.25 (m, 3H), 3.77 (s, 3H), 4.01 (s, 3H), 4.23–4.29 (m, 2H), 4.58 (d, ³*J*(H,H)=10.6 Hz, 1H), 6.04 (d, ³*J*(H,H)=10.6 Hz, 1H), 6.58 (d, ³*J*(H,H)=8.6 Hz, 1H), 7.07 (d, ³*J*(H,H)=8.6 Hz, 2H), 7.43 (s, 1H), 7.55 (s, 1H), 7.99 ppm (s, 1H); IR (KBr): $\tilde{\nu}=3489, 2960, 1718$ cm⁻¹; MS (70 eV): m/z (%): 329 (100) [*M*-BrC₆H₄CHCO₂C₂H₅]⁺; elemental analysis calcd (%) for C₃₁H₃₉O₅Br: C 65.14, H 6.88, N 0.00; found: C 64.85, H 6.94, N 0.00.

Ethyl 2-(4-bromophenyl)-3-(3,6-di-*tert*-butyl-2,7-dimethoxynaphthalen-1-yl)propanoate (10**):** The hydroxy ester **9** (630 mg, 1.10 mmol) was placed in a 30 mL round-bottomed flask and dissolved in CH₂Cl₂ (15 mL). Triethylsilane (0.26 mL, 1.65 mmol) and trifluoroacetic acid (0.37 mL, 4.85 mmol) were added to the mixture, which was stirred at room temperature for 1.5 h. After the addition of a satd. aqueous solution of NaHCO₃ (50 mL) to the reaction mixture, the mixture was extracted with ethyl acetate. The combined organic extracts were dried over Na₂SO₄, filtered, and concentrated under reduced pressure. The residue

was subjected to silica gel column chromatography with a 5:1 mixture of hexane and ethyl acetate as eluent to give the dehydroxylated compound **10** (584 mg, 96%) as an orange oil. M.p. 35°C; $R_f=0.50$ (5:1 hexane/ethyl acetate); $^1\text{H NMR}$ (270 MHz, CDCl_3): $\delta=1.33$ (s, 9H), 1.45 (s, 9H), 1.14 (m, 3H), 3.48–3.57 (m, 1H), 3.91–4.01 (m, 1H), 3.72 (s, 3H), 3.93 (s, 3H), 3.75–3.82 (m, 1H), 4.05–4.10 (m, 2H), 7.01 (d, $^3J(\text{H,H})=8.8$ Hz, 2H), 7.09 (s, 1H), 7.26 (d, $^3J(\text{H,H})=8.8$ Hz, 2H), 7.50 (s, 1H), 7.58 ppm (s, 1H); MS (70 eV): m/z (%): 554 (6) $[M]^+$, 552 (4) $[M]^+$, 313 (100) $[M-\text{BrC}_6\text{H}_4\text{CHCO}_2\text{C}_2\text{H}_5]^+$; elemental analysis calcd (%) for $\text{C}_{31}\text{H}_{39}\text{O}_4\text{Br}$: C 67.02, H 7.08, N 0.00; found: C 66.75, H 7.01, N, 0.00.

2-(4-Bromophenyl)-3-(3,6-di-tert-butyl-2,7-dimethoxynaphthalen-1-yl)propanoic acid (11): The ester **10** (1.18 g, 2.12 mmol) was placed in a 100 mL round-bottomed flask and dissolved in EtOH (40 mL). An aqueous solution (20 mL) of KOH (1.13 g, 20.1 mmol) was added to the mixture and heated at reflux under argon for 5 h. The reaction mixture was cooled to room temperature and then a 2 M HCl aqueous solution was added. The mixture was extracted with ethyl acetate and the organic layer dried over Na_2SO_4 , filtered, and concentrated under reduced pressure. The residue was subjected to silica gel column chromatography with a 10:1–1:1 mixture of hexane and ethyl acetate as eluent to give **11** (837 mg, 75%) as a pale-yellow solid. M.p. 91–92°C; $R_f=0.34$ (5:1 hexane/ethyl acetate); $^1\text{H NMR}$ (270 MHz, CDCl_3): $\delta=1.32$ (s, 9H), 1.45 (s, 9H), 3.71 (s, 3H), 3.93 (s, 3H), 3.52–3.61 (m, 1H), 3.74–3.84 (m, 1H), 4.04–4.08 (m, 1H), 7.01 (d, $^3J(\text{H,H})=8.4$ Hz, 2H), 7.28 (d, $^3J(\text{H,H})=8.4$ Hz, 2H), 7.10 (s, 1H), 7.50 (s, 1H), 7.59 ppm (s, 1H); IR (KBr): $\tilde{\nu}=3700$ –2400, 2957, 1709 cm^{-1} ; MS (70 eV): m/z (%): 528 (6) $[M]^+$, 526 (7) $[M]^+$, 313 (100) $[M-\text{BrC}_6\text{H}_4\text{CHCO}_2\text{C}_2\text{H}_5]^+$; elemental analysis calcd (%) for $\text{C}_{29}\text{H}_{35}\text{O}_4\text{Br}$: C 66.03, H 6.69, N 0.00; found: C 65.83, H 6.66, N 0.00.

2-(4-Bromophenyl)-5,8-di-tert-butyl-4,9-dimethoxyphenalane (12): The acid **11** (837 mg, 1.59 mmol) was placed in a 100 mL round-bottomed flask and mixed with oxalyl chloride (5 mL, 57 mmol). After stirring at 65°C for 4 h under argon, the reaction mixture was cooled to room temperature. Excess oxalyl chloride was then removed by distillation under reduced pressure and the residue was dissolved in CH_2Cl_2 (5 mL) and concentrated under reduced pressure (twice). After dissolving the residual oil in CH_2Cl_2 (40 mL) and cooling to -78°C , AlCl_3 (757 mg, 5.52 mmol) was added and the mixture stirred for 3.5 h under argon. It was then poured into a 2 M HCl aqueous solution (50 mL). The organic layer was separated and dried over Na_2SO_4 , filtered, and concentrated under reduced pressure. The residue was subjected to silica gel column chromatography with a 5:1 mixture of hexane and ethyl acetate as eluent to give the phenalane **12** (631 mg, 78%) as an orange powder. M.p. 75–76°C; $R_f=0.51$ (5:1 hexane/ethyl acetate); $^1\text{H NMR}$ (270 MHz, CDCl_3): $\delta=1.46$ (s, 9H), 1.49 (s, 9H), 3.81 (s, 3H), 3.83 (s, 3H), 3.56–3.79 (m, 2H), 4.05–4.14 (m, 1H), 7.13 (d, $^3J(\text{H,H})=8.6$ Hz, 2H), 7.43 (d, $^3J(\text{H,H})=8.6$ Hz, 2H), 7.63 (s, 1H), 7.90 ppm (s, 1H); IR (KBr): $\tilde{\nu}=2957$, 1697 cm^{-1} ; MS (70 eV) m/z (%): 510 (74) $[M]^+$, 508 (74) $[M]^+$; elemental analysis calcd (%) for $\text{C}_{29}\text{H}_{33}\text{O}_3\text{Br}$: C 68.36, H 6.53, N 0.00; found: C 67.99, H 6.50, N 0.00.

8-(4-Bromophenyl)-2,5-di-tert-butyl-6-hydroxyphenalene (13): The phenalane **12** (626 mg, 1.23 mmol) was placed in a 100 mL round-bottomed flask and dissolved in THF (20 mL). LiAlH_4 (164 mg, 4.32 mmol) was added to the mixture and stirred at room temperature for 20 min. It was then poured into 0.1 M phosphate buffer (pH 7) and vigorously stirred. The mixture was extracted with ethyl acetate and the organic extracts dried over Na_2SO_4 , filtered, and concentrated under reduced pressure. The residue was subjected to silica gel column chromatography with a 40:1–2:1 mixture of hexane and ethyl acetate as eluent to give phenalane derivatives as a mixture of diastereomers (510 mg, 81%).

Characterization data for the more polar diastereomer: yellow powder; m.p. 93–95°C; $R_f=0.19$ (5:1 hexane/ethyl acetate); $^1\text{H NMR}$ (270 MHz, CDCl_3): $\delta=1.48$ (s, 9H), 1.49 (s, 9H), 3.08–3.30 (m, 2H), 3.55–3.66 (m, 1H), 3.92 (s, 3H), 4.03 (s, 3H), 4.08–4.14 (m, 1H), 5.42–5.44 (m, 1H), 7.44 (d, $^3J(\text{H,H})=8.6$ Hz, 2H), 7.55 (d, $^3J(\text{H,H})=8.6$ Hz, 2H), 7.61 (s, 1H), 7.73 ppm (s, 1H).

Characterization data for the less polar diastereomer: yellow powder; m.p. 100–102°C; $R_f=0.44$ (5:1 hexane/ethyl acetate); $^1\text{H NMR}$ (270 MHz, CDCl_3): $\delta=1.47$ (s, 9H), 1.47 (s, 9H), 3.11–3.20 (m, 2H), 3.45 (m, 1H),

3.79 (s, 3H), 3.87 (s, 3H), 4.59 (s, 1H), 5.47 (d, $^3J(\text{H,H})=8.4$ Hz, 1H), 7.24 (m, 2H), 7.47 (d, $^3J(\text{H,H})=8.4$ Hz, 2H), 7.58 (s, 1H), 7.67 ppm (s, 1H); MS (70 eV) (mixture of diastereomers), m/z (%): 512 (85) $[M]^+$, 510 (100) $[M]^+$.

The phenalane (mixture of diastereomers, 380 mg, 0.74 mmol) was placed in a 20 mL round-bottomed flask and dissolved in HMPA (10 mL). LiI (1.99 g, 14.9 mmol) was added to the mixture and stirred at 170°C for 6 h. It was then cooled to room temperature and poured into a 2 M HCl aqueous solution. The mixture was extracted with ethyl acetate and the organic layer was dried over Na_2SO_4 , filtered, and concentrated under reduced pressure. The residue was subjected to deactivated silica gel column chromatography with a 10:1–1:1 mixture of hexane and ethyl acetate as eluent to give the hydroxyphenalene **13** (280 mg, 64%) as a vivid reddish-orange powder. M.p. 200–202°C; $R_f=0.39$ (5:1 hexane/ethyl acetate); $^1\text{H NMR}$ (270 MHz, CDCl_3): $\delta=1.53$ (s, 18H), 7.47 (brs, 4H), 7.65 (brs, 2H), 8.63 ppm (brs, 2H); IR (KBr): $\tilde{\nu}=2930$ cm^{-1} ; IR (CCl_2CCl_2): $\tilde{\nu}=3629$, 2958 cm^{-1} ; MS (70 eV): m/z (%): 464 (27) $[M]^+$, 462 (29) $[M]^+$, 407 (90%) $[M-\text{C}(\text{CH}_3)_3]^+$, 405 (100) $[M-\text{C}(\text{CH}_3)_2]^+$; elemental analysis calcd (%) for $\text{C}_{27}\text{H}_{27}\text{O}_2\text{Br}$: C 69.98, H 5.87, N 0.00; found: C 69.79, H 5.78, N 0.00.

8-(4-Bromophenyl)-2,5-di-tert-butyl-6-oxophenalenoxy (7): The hydroxyphenalene **13** (32 mg, 0.068 mmol) was placed in a 50 mL round-bottomed flask and dissolved in benzene (5 mL, degassed by argon bubbling for 2 h prior to use). PbO_2 (33 mg, 0.14 mmol) was added to the mixture and stirred for 15 min. It was then filtered through Celite and the filtrate concentrated in vacuo to give the π radical **7**. M.p. 273–275°C (decomp.); $R_f=0.39$ (5:1 hexane/ethyl acetate); IR (KBr): $\tilde{\nu}=2958$, 1715, 1594 cm^{-1} ; UV/Vis (KBr): $\lambda_{\text{max}}=704$, 424, 255 nm; UV/Vis (hexane): $\lambda_{\text{max}}=650$, 503, 415, 392, 269 nm; elemental analysis calcd (%) for $(\text{C}_{27}\text{H}_{26}\text{O}_2\text{Br})\cdot((\text{CH}_3)_2\text{CO})$: C 69.23, H 6.20, N 0.00; found: C 68.96, H 6.04, N 0.00.

A single crystal, including acetone as a solvent of crystallization, suitable for X-ray crystal structure analysis was obtained as a black block by the following method: The π radical **7** (10.5 mg), CHCl_3 (0.5 mL), and acetone (2.5 mL) were placed at a glass tube previously filled with argon. The solution was degassed by a repeated freeze–pump–thaw method (seven times). After sealing the glass tube, the solution was allowed to stand at -20°C . The resulting crystals were filtered off in air;

Recrystallization of 2,5,8-tri-tert-butyl-6-oxophenalenoxy (1): The π radical **1** (19 mg) and hexane (4 mL) were placed in a glass tube previously filled with argon. The solution was degassed by a repeated freeze–pump–thaw method (seven times). After sealing the glass tube, the solution was allowed to stand at -20°C . The resulting crystals were obtained as a black block by filtration in air.

8-(4-Iodophenyl)-2,5-di-tert-butyl-6-oxophenalenoxy (2): 8-(4-Iodophenyl)-2,5-di-tert-butyl-6-hydroxyphenalene^[9] (28 mg, 0.055 mmol) was placed in a 30 mL round-bottomed flask and dissolved in CH_2Cl_2 (10 mL). An excess amount of PbO_2 (57 mg, 0.24 mmol) was added to the mixture and stirred for 10 min. The mixture was then filtered through Celite and the filtrate concentrated in vacuo to give the π radical **2** (24 mg, 86%) as a deep-green powder. M.p. 215–217°C (decomp.); $R_f=0.39$ (5:1 hexane/ethyl acetate); IR (KBr): $\tilde{\nu}=2958$, 1595 cm^{-1} ; UV/Vis (KBr): $\lambda_{\text{max}}=680$, 426, 268 nm; UV/Vis (hexane): $\lambda_{\text{max}}=651$, 415, 392, 270 nm; elemental analysis (powder) calcd (%) for $\text{C}_{27}\text{H}_{26}\text{O}_2\text{I}$: C 63.66, H 5.14, N 0.00; found: C 63.75, H 5.15, N 0.00.

Single crystals including acetonitrile as a solvent of crystallization suitable for X-ray crystal structure analysis were obtained as green blocks by the following method: The π radical **2** (3 mg), acetonitrile (1 mL), and hexane (4 mL) were placed at a glass tube previously filled with argon. The solution was degassed by a repeated freeze–pump–thaw method (eight times). After sealing the glass tube, the solution was allowed to stand at 4°C. The resulting crystals were filtered in air.

Crystal data for 1: $\text{C}_{25}\text{H}_{31}\text{O}_2$, $M_r=363.50$, cubic, $a=20.2890$ Å, $V=8351(7)$ Å³, $T=200$ K, space group $Ia\bar{3}$ (#206), $Z=16$, 25088 reflections measured, 1602 independent reflections ($R_{\text{int}}=0.126$), which were used in all calculations. The final $wR(F^2)$ value was 0.2058 (all data).

Crystal data for 2-(CH₃CN): $(\text{C}_{27}\text{H}_{26}\text{O}_2\text{I})(\text{CH}_3\text{CN})_{0.64}$, $M_r=535.79$, monoclinic, $a=12.5389(9)$, $b=8.3309(5)$, $c=24.5593(12)$ Å, $\beta=101.6940(10)^\circ$,

$V=2512.2(3) \text{ \AA}^3$, $T=200 \text{ K}$, space group $P2_1/n$ (#14), $Z=4$, 18120 reflections measured, 5697 independent reflections ($R_{\text{int}}=0.043$), which were used in all calculations. The final $wR(F^2)$ value was 0.173 (all data).

Crystal data for 7-((CH₃)₂CO): (C₂₇H₂₆O₂Br)(C₅H₆O), $M_r=520.48$, monoclinic, $a=12.8650(7)$, $b=17.102(1)$, $c=12.228(1) \text{ \AA}$, $\beta=107.661(3)^\circ$, $V=2563.5(4) \text{ \AA}^3$, $T=200 \text{ K}$, space group $C2m$ (#12), $Z=4$, 11359 reflections measured, 3039 independent reflections ($R_{\text{int}}=0.0652$), which were used in all calculations. The final $wR(F^2)$ value was 0.142 (all data).

CCDC-238265 (for **1**), CCDC-938325 (for **2**-(CH₃CN)), and CCDC-238266 (for **7**-(CH₃)₂CO) contain the supplementary crystallographic data for this paper. These data can be obtained free of charge from The Cambridge Crystallographic Data Centre via www.ccdc.cam.ac.uk/data_request/cif.

Acknowledgements

This work was partially supported by grants from the Yazaki Memorial Foundation for Science and Technology, The Japan Securities Scholarship Foundation, Kansai Research Foundation for Technology Promotion, a Grant-in-Aid for Scientific Research on Innovative Areas (No. 20110006 and Quantum Cybernetics), the Elements Science and Technology Project of the Ministry of Education, Culture, Sports, Science and Technology, Japan, and the Core Research For Evolutional Science and Technology (CREST) of the Japan Science and Technology Agency.

- [1] For overviews of stable open-shell organic molecules, see: a) A. R. Forrester, J. M. Hay, R. H. Thomson, *Organic Chemistry of Stable Free Radicals*, Academic Press, London, **1968**; b) R. G. Hicks, *Org. Biomol. Chem.* **2007**, *5*, 1321–1338; c) *Stable Radicals: Fundamentals and Applied Aspects of Odd-Electron Compounds* (Ed.: R. G. Hicks), Wiley, Chichester, **2010**.
- [2] a) *Magnetic Properties of Organic Materials* (Ed.: P. M. Lahti), Marcel Dekker, New York, **1999**; b) *Molecular Magnetism* (Eds.: K. Itoh, M. Kinoshita), Kodansha, Gordon, and Breach, Tokyo, **2000**; c) K. Itoh, T. Takui, *Proc. Jpn. Acad. Ser. B* **2004**, *80*, 29–40; d) T. Takui, K. Itoh, *Chem. Phys. Lett.* **1973**, *19*, 120–124; e) Y. Teki, T. Takui, K. Itoh, H. Iwamura, K. Kobayashi, *J. Am. Chem. Soc.* **1986**, *108*, 2147–2156; f) I. Fujita, Y. Teki, T. Takui, T. Kinoshita, K. Itoh, F. Miko, T. Sawaki, H. Iwamura, A. Izuoka, T. Sugawara, *J. Am. Chem. Soc.* **1990**, *112*, 4074–4075; g) Y. Teki, I. Fujita, T. Takui, T. Konoshita, K. Itoh, *J. Am. Chem. Soc.* **1994**, *116*, 11499–11505; h) K. Sato, M. Yano, M. Furuichi, D. Shiomi, T. Takui, K. Abe, K. Itoh, A. Higuchi, K. Katsuma, Y. Shirota, *J. Am. Chem. Soc.* **1997**, *119*, 6607–6613; i) D. Shiomi, M. Nishizawa, K. Sato, T. Takui, K. Itoh, H. Sakurai, A. Izuoka, T. Sugawara, *J. Phys. Chem. B* **1997**, *101*, 3342–3348.
- [3] For recent studies of molecular spin quantum computing by pulsed ENDOR and ELDOR techniques, see: a) R. Rahimi, K. Sato, D. Shiomi, T. Takui, in *Modern Magnetic Resonance* (Ed.: G. A. Webb), Springer, Heidelberg, **2007**, pp. 643–650; b) K. Sato, S. Nakazawa, R. Rahimi, T. Ise, S. Nishida, T. Yoshino, N. Mori, K. Toyota, D. Shiomi, Y. Yakiyama, Y. Morita, M. Kitagawa, K. Nakasuji, M. Nakahara, H. Hara, P. Carl, P. Höfer, T. Takui, *J. Mater. Chem.* **2009**, *19*, 3739–3754; c) K. Sato, S. Nakazawa, R. D. Rahimi, S. Nishida, T. Ise, D. Shiomi, K. Toyota, Y. Morita, M. Kitagawa, P. Carl, P. Höfer, T. Takui, in *Molecular Realizations of Quantum Computing 2007* (Eds.: M. Nakahara, Y. Ota, R. Rahimi, Y. Kondo, M. Tada-Umezaki), Kinki University Series on Quantum Computing, World Scientific, **2009**, pp. 58–162; d) Y. Morita, Y. Yakiyama, S. Nakazawa, T. Murata, T. Ise, D. Hashizume, D. Shiomi, K. Sato, M. Kitagawa, K. Nakasuji, T. Takui, *J. Am. Chem. Soc.* **2010**, *132*, 6944–6946; e) T. Yoshino, S. Nishida, K. Sato, S. Nakazawa, R. D. Rahimi, K. Toyota, D. Shiomi, Y. Morita, M. Kitagawa, T. Takui, *J. Phys. Chem. Lett.* **2011**, *2*, 449–453; f) Y. Yakiyama, T. Murata, T. Ise, D. Shiomi, K. Sato, T. Takui, K. Nakasuji, Y. Morita, *Eur. J. Inorg. Chem.* **2011**, 3438–3445; g) K. Ayabe, K. Sato, S. Nishida, T. Ise, S. Nakazawa, K. Sugisaki, Y. Morita, K. Toyota, D. Shiomi, M. Kitagawa, T. Takui, *Phys. Chem. Chem. Phys.* **2012**, *14*, 9137–9148; h) S. Nakazawa, S. Nishida, T. Ise, T. Yoshino, N. Mori, R. Rahimi, K. Sato, Y. Morita, K. Toyota, D. Shiomi, M. Kitagawa, H. Hara, P. Carl, P. Höfer, T. Takui, *Angew. Chem.* **2012**, *124*, 9998–10002; *Angew. Chem. Int. Ed.* **2012**, *51*, 9860–9864; i) “Novel Applications of EPR/EPR: Quantum Computing/Quantum Information Processing” K. Sato, S. Nakazawa, S. Nishida, R. D. Rahimi, T. Yoshino, Y. Morita, K. Toyota, D. Shiomi, M. Kitagawa, T. Takui, in *EPR of Free Radicals in Solids II, Progress in Theoretical Chemistry and Physics Volume 25* (Eds.: A. Lund, M. Shiotani), Springer, Dordrecht, pp. 163–204, **2013**; j) A. Ueda, S. Suzuki, K. Yoshida, K. Fukui, K. Sato, T. Takui, K. Nakasuji, Y. Morita, *Angew. Chem.* **2013**, *125*, 4895–4899; *Angew. Chem. Int. Ed.* **2013**, *52*, 4795–4799.
- [4] a) J. Casado, P. M. Burrezo, F. J. Ramírez, J. T. L. Navarrete, S. H. Lapidus, P. W. Stephens, H.-L. Vo, J. S. Miller, F. Mota, J. J. Novoa, *Angew. Chem.* **2013**, *125*, 6549–6553; *Angew. Chem. Int. Ed.* **2013**, *52*, 6421–6425; b) J. S. Miller, J. J. Novoa, *Acc. Chem. Res.* **2007**, *40*, 189–196; c) R. E. Del Sesto, J. S. Miller, P. Lafuente, J. J. Novoa, *Chem. Eur. J.* **2002**, *8*, 4894–4908; d) J. J. Novoa, P. Lafuente, R. E. Del Sesto, J. S. Miller, *Angew. Chem.* **2001**, *113*, 2608–2613; *Angew. Chem. Int. Ed.* **2001**, *40*, 2540–2545.
- [5] a) For phenalenyl as a potential building block for molecular conductors, see: R. C. Haddon, *Nature* **1975**, *256*, 394–396; b) the first phenalenyl-based single-component molecular conductor, see: X. Chi, M. E. Itkis, B. O. Patrick, T. M. Barclay, R. W. Reed, R. T. Oakley, A. W. Cordes, R. C. Haddon, *J. Am. Chem. Soc.* **1999**, *121*, 10395–10402; c) for application to molecular spin memory devices, see: K. V. Raman, A. M. Kamerbeek, A. Mukherjee, N. Atodiresei, T. K. Sen, P. Lazić, V. Caciuc, R. Michel, D. Stalke, S. K. Mandal, S. Blügel, M. Müntenberg, J. S. Moodera, *Nature* **2013**, *493*, 509–513.
- [6] For a recent comprehensive overview on phenalenyl systems, see: a) “Phenalenyls, Cyclopentadienyls, and Other Carbon-Centered Radicals”: Y. Morita, S. Nishida, in *Stable Radicals: Fundamentals and Applied Aspects of Odd-Electron Compounds* (Ed.: R. G. Hicks), Wiley, Chichester, **2010**, Chapter 3, pp. 81–145; b) Y. Morita, S. Suzuki, K. Sato, T. Takui, *Nat. Chem.* **2011**, *3*, 197–204; c) Y. Morita, S. Nishida, T. Takui, K. Nakasuji, *J. Synth. Org. Chem. Jpn.* **2012**, *70*, 50–59.
- [7] K. Goto, T. Kubo, K. Yamamoto, K. Nakasuji, K. Sato, D. Shiomi, T. Takui, M. Kubota, T. Kobayashi, K. Yakushi, J. Ouyang, *J. Am. Chem. Soc.* **1999**, *121*, 1619–1620.
- [8] For the π dimer of the dithiophenalenyl radical, see: a) R. C. Haddon, F. Wudl, M. L. Kaplan, J. H. Marshall, R. E. Cais, F. B. Bramwell, *J. Am. Chem. Soc.* **1978**, *100*, 7629–7633; b) L. Beer, S. K. Mandal, R. W. Reed, R. T. Oakley, F. S. Tham, B. Donnadieu, R. C. Haddon, *Cryst. Growth Des.* **2007**, *7*, 802–809.
- [9] For the π dimeric structure of a phenalenyl-based singlet biradicaloid, see: T. Kubo, A. Shimizu, M. Sakamoto, M. Uruichi, K. Yakushi, M. Nakano, D. Shiomi, K. Sato, T. Takui, Y. Morita, K. Nakasuji, *Angew. Chem.* **2005**, *117*, 6722–6726; *Angew. Chem. Int. Ed.* **2005**, *44*, 6564–6568.
- [10] S. Suzuki, Y. Morita, K. Fukui, K. Sato, D. Shiomi, T. Takui, K. Nakasuji, *J. Am. Chem. Soc.* **2006**, *128*, 2530–2531.
- [11] Kochi termed the long C–C bond in the π dimer of TBPLY a 12-centered covalent bond, see: a) D. Small, V. Zaitsev, Y. Jung, S. V. Rosokha, M. Head-Gordon, J. K. Kochi, *J. Am. Chem. Soc.* **2004**, *126*, 13850–13858; b) S. V. Rosokha, J. Zhang, J. Lu, J. K. Kochi, *J. Phys. Org. Chem.* **2010**, *23*, 395–399.
- [12] a) X. Chi, M. E. Itkis, K. Kirschbaum, A. A. Pinkerton, R. T. Oakley, A. W. Cordes, R. C. Haddon, *J. Am. Chem. Soc.* **2001**, *123*, 4041–4048; b) M. E. Itkis, X. Chi, A. W. Cordes, R. C. Haddon, *Science* **2002**, *296*, 1443–1445.
- [13] Y. Morita, T. Aoki, K. Fukui, S. Nakazawa, K. Tamaki, S. Suzuki, A. Fuyuhiko, K. Yamamoto, K. Sato, D. Shiomi, A. Naito, T. Takui, K.

- Nakasuji, *Angew. Chem.* **2002**, *114*, 1871–1874; *Angew. Chem. Int. Ed.* **2002**, *41*, 1793–1796.
- [14] For the first continuous color change with temperature of a crystal as a single-component material, see: Y. Morita, S. Suzuki, K. Fukui, S. Nakazawa, H. Kitagawa, H. Kishida, H. Okamoto, A. Naito, A. Sekine, Y. Ohashi, M. Shiro, K. Sasaki, D. Shiomi, K. Sato, T. Takui, K. Nakasuji, *Nat. Mater.* **2008**, *7*, 48–51.
- [15] Y. Morita, T. Ohba, N. Haneda, S. Maki, J. Kawai, K. Hatanaka, K. Sato, D. Shiomi, T. Takui, K. Nakasuji, *J. Am. Chem. Soc.* **2000**, *122*, 4825–4826.
- [16] 2,5-Dimethyl-6-oxophenalenoxyl affords σ -dimeric compounds, see: K. Hatanaka, Y. Morita, T. Ohba, K. Yamaguchi, T. Takui, M. Kinoshita, K. Nakasuji, *Tetrahedron Lett.* **1996**, *37*, 877–880.
- [17] Y. Morita, J. Kawai, K. Fukui, S. Nakazawa, K. Sato, D. Shiomi, T. Takui, K. Nakasuji, *Org. Lett.* **2003**, *5*, 3289–3291.
- [18] This redox-dependent spin nature was termed redox-based spin diversity, see: a) Y. Morita, S. Nishida, J. Kawai, K. Fukui, S. Nakazawa, K. Sato, D. Shiomi, T. Takui, K. Nakasuji, *Org. Lett.* **2002**, *4*, 1985–1988; b) Y. Morita, S. Nishida, J. Kawai, T. Takui, K. Nakasuji, *Pure Appl. Chem.* **2008**, *80*, 507–517.
- [19] a) Y. Morita, J. Kawai, S. Nishida, N. Haneda, K. Fukui, K. Sato, D. Shiomi, T. Takui, K. Nakasuji, *Synth. Met.* **2003**, *137*, 1217–1218; b) Synthetic method of the radical precursor of **2**: Y. Morita, J. Kawai, N. Haneda, S. Nishida, K. Fukui, S. Nakazawa, D. Shiomi, K. Sato, T. Takui, T. Kawakami, K. Yamaguchi, K. Nakasuji, *Tetrahedron Lett.* **2001**, *42*, 7991–7995.
- [20] S. Nishida, K. Kariyazono, A. Yamanaka, K. Fukui, K. Sato, T. Takui, K. Nakasuji, Y. Morita, *Chem. Asian J.* **2011**, *6*, 1188–1196.
- [21] For 7-hydroxy-2,5,8-tri-*tert*-butyl-6-oxophenalenoxyl with a strong intramolecular hydrogen-bonding interaction, see: Y. Morita, S. Maki, K. Fukui, T. Ohba, J. Kawai, K. Sato, D. Shiomi, T. Takui, K. Nakasuji, *Org. Lett.* **2001**, *3*, 3099–3102.
- [22] S. Nishida, Y. Morita, K. Fukui, K. Sato, D. Shiomi, T. Takui, K. Nakasuji, *Angew. Chem.* **2005**, *117*, 7443–7446; *Angew. Chem. Int. Ed.* **2005**, *44*, 7277–7280.
- [23] For high-capacity secondary batteries using **1**, see: a) Y. Morita, S. Nishida, T. Murata, M. Moriguchi, A. Ueda, M. Satoh, K. Arifuku, K. Sato, T. Takui, *Nat. Mater.* **2011**, *10*, 947–951; b) Y. Morita, T. Okafuji, M. Satoh, *Jpn. Kokai Tokkyo Koho*, JP 2007227186 A, **2007**; c) for the use of closed-shell organic acceptors/donors as cathode-active materials, see: S. Nishida, Y. Yamamoto, T. Takui, Y. Morita, *ChemSusChem* **2013**, *6*, 794–797.
- [24] Gaussian 03, Revision E.01, M. J. Frisch, G. W. Trucks, H. B. Schlegel, G. E. Scuseria, M. A. Robb, J. R. Cheeseman, J. A. Montgomery, Jr., T. Vreven, K. N. Kudin, J. C. Burant, J. M. Millam, S. S. Iyengar, J. Tomasi, V. Barone, B. Mennucci, M. Cossi, G. Scalmani, N. Rega, G. A. Petersson, H. Nakatsuji, M. Hada, M. Ehara, K. Toyota, R. Fukuda, J. Hasegawa, M. Ishida, T. Nakajima, Y. Honda, O. Kitao, H. Nakai, M. Klene, X. Li, J. E. Knox, H. P. Hratchian, J. B. Cross, V. Bakken, C. Adamo, J. Jaramillo, R. Gomperts, R. E. Stratmann, O. Yazyev, A. J. Austin, R. Cammi, C. Pomelli, J. W. Ochterski, P. Y. Ayala, K. Morokuma, G. A. Voth, P. Salvador, J. J. Dannenberg, V. G. Zakrzewski, S. Dapprich, A. D. Daniels, M. C. Strain, O. Farkas, D. K. Malick, A. D. Rabuck, K. Raghavachari, J. B. Foresman, J. V. Ortiz, Q. Cui, A. G. Baboul, S. Clifford, J. Cio-slowski, B. B. Stefanov, G. Liu, A. Liashenko, P. Piskorz, I. Komaromi, R. L. Martin, D. J. Fox, T. Keith, M. A. Al-Laham, C. Y. Peng, A. Nanayakkara, M. Challacombe, P. M. W. Gill, B. Johnson, W. Chen, M. W. Wong, C. Gonzalez, J. A. Pople, Gaussian, Inc., Wallingford CT, **2004**.
- [25] A quasi-imposed stacking trimer of perchlorophenalenyl has a long intermolecular distance (3.78 Å) due to the nonplanarity of the phenalenyl skeleton arising from the steric repulsion of chlorine atoms at the *peri* positions, see: a) R. C. Haddon, S. V. Chichester, S. M. Stein, J. H. Marshall, A. M. Mujsce, *J. Org. Chem.* **1987**, *52*, 711–712; b) P. A. Koutentis, Y. Chen, Y. Cao, T. P. Best, M. E. Itkis, L. Beer, R. T. Oakley, A. W. Cordes, C. P. Brock, R. C. Haddon, *J. Am. Chem. Soc.* **2001**, *123*, 3864–3871.
- [26] Acetonitrile is present as solvent of crystallization and has no contact with molecule **2** within the sum of the van der Waals radii.
- [27] Acetone is present as solvent of crystallization and has no contact with molecule **7** within the sum of the van der Waals radii.
- [28] a) P. v. R. Schleyer, C. Maerker, A. Dransfeld, H. Jiao, N. J. R. v. E. Hommes, *J. Am. Chem. Soc.* **1996**, *118*, 6317–6318; b) V. Gogonea, P. von R. Schleyer, P. R. Schreiner, *Angew. Chem.* **1998**, *110*, 2045–2049; *Angew. Chem. Int. Ed.* **1998**, *37*, 1945–1948.
- [29] Y. Morita, S. Nishida, J. Kawai, K. Fukui, S. Nakazawa, K. Sato, D. Shiomi, T. Takui, K. Nakasuji, *Polyhedron* **2003**, *22*, 2209–2213. Operation of the method was described in detail, see ref. 20.
- [30] The π dimer of TBPLY stacks in a herringbone motif without any interdimer interactions, see ref. [7].
- [31] Another conceivable factor for the small SOMO–SOMO interaction is the intermolecular steric repulsion between the oxygen atoms and *tert*-butyl groups; the conformation of the *tert*-butyl groups of **1** is considerably restricted by adjacent oxygen atoms, inhibiting the rotation of *tert*-butyl groups to release the steric repulsion of the oxygen atoms in the counter molecule. In fact, the close contacts (O–C distances: 2.94–3.10 Å) between the oxygen atoms and the methyl groups in the *tert*-butyl groups are within the sum of the van der Waals radii (3.22 Å). On the other hand, the *tert*-butyl groups in TBPLY can adopt conformations to minimize the steric repulsion of hydrogen atoms in the counter molecule.
- [32] In general, the π dimers of organic π radicals are characterized by intermolecular charge-transfer absorption bands, see: a) T. Sakata, S. Nagakura, *Bull. Chem. Soc. Jpn.* **1969**, *42*, 1497–1503; b) M. R. Gleiter, B. Kanellakopoulos, C. Krieger, F. A. Neugebauer, *Liebigs Ann.* **1997**, 473–483; c) J.-M. Lü, S. V. Rosokha, J. K. Kochi, *J. Am. Chem. Soc.* **2003**, *125*, 12161–12171; d) see ref. [10] and references therein.
- [33] The molar ratios of the diamagnetic and $S = 1/2$ impurities in the defects are assumed to be identical ($=\alpha$) to avoid overparametrization.
- [34] The exchange interaction of $2J$ is not an adjustable parameter in our analysis: Numerical differentiation of the first term in (1) with respect to T gives the temperature T_{\max} in which χ_p has a maximum, $T_{\max} = 1.247J/|k_B$, as a function of $|J|$. The maximum value of χ_p at T_{\max} is given as $\chi_{\max} = 0.07547g^2/(|J|/k_B)$. From these, the trajectory of a point (T_{\max}, χ_{\max}) for the ground-state singlet dimer is given by $\chi_{\max} = 0.09413g^2/T_{\max}$, which is independent of J . The exchange interaction of $2J/k_B = 384$ K has been fixed so as to reproduce the observed point of (T_{\max}, χ_{\max}).
- [35] Single crystals of **1** were obtained in very poor yield (<1%) in the recrystallization process.
- [36] Y. Takano, T. Taniguchi, H. Isobe, T. Kubo, Y. Morita, K. Yamamoto, K. Nakasuji, T. Takui, K. Yamaguchi, *J. Am. Chem. Soc.* **2002**, *124*, 11122–11130.
- [37] For the topological symmetry control of spin density distribution in organic polyradical systems for control of intramolecular exchange interactions, see: S. Nakazawa, K. Sato, D. Shiomi, M. Yano, T. Kinoshita, M. L. T. M. B. Franco, M. C. R. L. R. Lazana, M. C. B. L. Shohoji, K. Itoh, T. Takui, *Phys. Chem. Chem. Phys.* **2011**, *13*, 1424–1433.
- [38] Phenalenyl-fused corannulene and a corannulene bearing two phenoxyl radicals for three-dimensional intermolecular spin interaction through a curved π -conjugated system, see: a) S. Nishida, Y. Morita, A. Ueda, T. Kobayashi, K. Fukui, K. Ogasawara, K. Sato, T. Takui, K. Nakasuji, *J. Am. Chem. Soc.* **2008**, *130*, 14954–14955; b) A. Ueda, S. Nishida, K. Fukui, T. Ise, D. Shiomi, K. Sato, T. Takui, K. Nakasuji, Y. Morita, *Angew. Chem.* **2010**, *122*, 1722–1726; *Angew. Chem. Int. Ed.* **2010**, *49*, 1678–1682. For recent overview of bowl-shaped stable neutral radical, see: c) “Curved π -Conjugated Stable Open-shell Systems Possessing Three-dimensional Molecular/Electronic-spin Structures”: Y. Morita, A. Ueda, in *Fragments of Fullerenes and Carbon Nanotubes: Designed Synthesis Unusual Reactions, and Coordination Chemistry*, (Eds.: L. T. Scott, M. Petrukhina), Wiley, New Jersey, **2011**, Chapter 4, pp. 95–134.

- [39] For a [4]helicene-based chiral neutral π radical with a spin-delocalized nature, see: A. Ueda, H. Wasa, S. Suzuki, K. Okada, K. Sato, T. Takui, Y. Morita, *Angew. Chem.* **2012**, *124*, 6795–6799; *Angew. Chem. Int. Ed.* **2012**, *51*, 6691–6695.
- [40] For rioxotriangulene (TOT) as a two-dimensional π -extended 6OPO analogue, see reference [22]; for a TOT-based neutral π radical with three dicyanomethyl groups, see: A. Ueda, H. Wasa, S. Nishida, Y. Kanzaki, K. Sato, D. Shiomi, T. Takui, Y. Morita, *Chem. Eur. J.* **2012**, *18*, 16272–16276.
- [41] G. M. Sheldrick, SHELXL-97, Program for the Refinement of Crystal Structures, University of Göttingen, Göttingen 1997.
- [42] a) R. Kuhn, I. Hammer, *Chem. Ber.* **1950**, *83*, 413–414; b) W. K. Wilmarth, N. Schwartz, *J. Am. Chem. Soc.* **1955**, *77*, 4543–4551.

Received: May 9, 2013

Published online: ■■■, 0000